Engineering and Technology Journal
Journal homepage: https://etj.uotechnology.edu.iq

Fabrication of Silver Nanoparticles in Aqueous Solution by Laser Technique and Study of Their Hemocompatibility and Antibacterial Effects Against Dental Decay Bacteria

Ruaa H. Abbas[a], Azhar M. Haleem*[b], Abdulhadi K. Judran[a]

[a] Laser and Optoelectronics Engineering Dept., University of Technology-Iraq, Alsina'a street, 10066 Baghdad, Iraq.
[b] Environment Research Center, University of Technology-Iraq, Alsina'a street, 10066 Baghdad, Iraq.
*Corresponding author Email: amhjanabi74@gmail.com

HIGHLIGHTS

- The ablation with a Q-switched Nd:YAG laser (1064 nm, 600 mJ at room temperature, a pulse duration of 10 ns, and a repetition rate of 5 Hz.) was capable of preparing spherical graphitic shape of Ag NPs.
- Ablation in CTAB liquids results in spherical particles of Ag NPs with a particle size distribution ranging from (5-70 nm) and an absorption spectrum around 425 nm.
- The in vitro assay revealed that prepared Ag NPs have significant antibacterial activity against Streptococcus mutans and moderate toxic effects at high concentrations, with the hemolysis rate of red blood cells.

ARTICLE INFO

Handling editor: Makram A. Fakhri

Keywords:

Ag NPs
Laser ablation
Streptococcus mutans
Antibacterial activity
Red blood cells

ABSTRACT

In the current work, silver nanoparticles (Ag-NPs) were successfully synthesized via laser ablation while their hemocompatibility and antibacterial features were tested against dental decay bacteria. The silver bulk was immersed in cetrimonium bromide (CTAB) and focused by a pulsed Nd:YAG laser at 1064 nm, 600 mJ at room temperature, a pulse duration of 10 ns, and a repetition rate of 5 Hz. The obtained Ag-NPs suspension was systematically and comprehensively characterized by harnessing UV–Vis spectroscopy, zeta potential (ZP), Fourier transform infrared (FTIR), X-ray diffraction (XRD), field emission scanning electron microscopy (FESEM), and transmission electron microscopy (TEM). Results demonstrated that the absorption spectrum of Ag NPs colloidal solution was characterized by the peak observed at 425 nm. Meanwhile, The NPs XRD patterns revealed the presence of Ag phase planes (111), (200), and (220). All samples manifested aggregation-induced spherical nanostructures as disclosed by the FESEM images. Besides, the TEM images revealed nearly spherical NPs, with sizes ranging from 5–70 nm, for Ag NPs prepared with CTAB. The antibacterial activity against a clinical isolate of Streptococcus mutans was conducted at a wide spectrum Ag concentration range (0.0, 50, 75, 100, and 200) µg/mL. The in vitro hemocompatibility effects were obtained by measuring the hemolysis rate of red blood cells. Results reported that the antibacterial activity against Streptococcus mutans was size and concentration-dependent, and the hemolysis rate revealed low effects at low concentrations. Thus, Ag NPs could be a promising candidates to treat and prevent dental caries.

1. Introduction

Nanotechnology has been proposed as a promising technological field for wide-spectrum applications. Environmental protection, materials, packaging, and medical devices are just a few of the applications for metal nanoparticles. Among the presently available nanomaterials harnessed for biomedical applications, metal nanoparticles (MNPs) demonstrated a promising potential to behave as pharmacological agent transporters [1, 2]. Nanoparticles have been used in medicine as monoclonal antibodies, enzymes, and bioactive molecules. Previously, polymeric and nanoparticles made up of both metals and nonmetals have been employed [3]. In this context, silver nanoparticles (Ag NPs) are one of the most frequently studied nanoparticles. This was attributed to their high aspect ratio (surface-to-volume ratio), low cost, cytotoxicity, immunological

http://doi.org/10.30684/etj.2023.136922.1329
Received 13 November 2022; Accepted 05 January 2023; Available online 11 January 2023
2412-0758/University of Technology-Iraq, Baghdad, Iraq

response, and antimicrobial activity even at low concentrations. This wide range of Ag-NPs potential has made these nanoparticles a preferable choice in biomedical applications [1, 4].

Ag NPs have been utilized in dentistry to synthesise antimicrobial compounds aiming to enhance the quality of dental products for better treatment outcomes [5]. They can be integrated into a wide range of dental care products, including composite and acrylic resins for direct restoration, endodontic irrigants and obturating materials, orthodontic adhesives, gingival membranes for assisted tissue regeneration, and titanium coats for dental implants [5, 6]. In recent years, the frequency of biological and bacterial infection instances at companies that produce or handle consumable items such as food and water has risen. Scientists have created non-toxic, user-friendly inorganic antibacterial nanomaterials in response to this rising concern [7, 8].

Certain materials, like metal oxide semiconductors, can create entirely new materials with novel electronic and optical properties when they are downsized to extremely small dimensions [9–11]. The main factors influencing the shape and size of nanoscale materials that can be created by laser ablation in liquid are the laser's power, wavelength, and pulse length [12–14]. The acute disease known as caries is brought on by the presence of harmful bacteria in the oral cavity. oral mucosal streptococci, especially S. mutans. The main contributor to microbial species or biofilm and the start of dental caries is the activity of the enzyme glucosyltransferase (GTFase), which is produced by biofilm bacteria, particularly Streptococcus mutans. Caries is an acute disease brought on by the presence of harmful bacteria in the oral cavity. Streptococci which thus affect the oral mucosa, especially S. mutans. The major contributor to microbial species or biofilm and the onset of dental caries is the activity of glucosyltransferase (GTFase), which is particularly active in Streptococcus mutans biofilm bacteria. GTFase produces acid and insoluble glucan in water.Comparatively few studies have looked at how these bacteria interact with metal-containing nanoparticles (NPs) compared to other microbe groups [15, 16].

Recent studies have demonstrated that blue light can kill a variety of microorganisms, including some that are drug-resistant. In addition, there is mounting proof that Ag NPs are more effective at eradicating germs when exposed to blue light. As a result, both Gram-positive and Gram-negative bacteria are eliminated. These results demonstrate that a lower concentration of Ag NPs is necessary to kill bacteria, which lessens the risk of Ag NPs toxicity [17, 18]. Resistance to antimicrobial drugs is a key factor in this occurrence. It suggests that smaller nanoparticles can penetrate bacteria more effectively. Nanoparticles are more likely to interact with surfaces and cause harm if they have a positive zeta potential and a small diameter [19]. Electrostatic forces are created when positively charged nanoparticles collide, bringing together microorganisms with opposingly charged surfaces and increasing their attraction to one another [20–22]. For the treatment of early dental caries, numerous studies have suggested the use of silver nanoparticles in a variety of preparations [18, 19]. Strong antimicrobial agents, silver nanoparticles are effective in vitro against cariogenic bacteria like Streptococcus mutans. They are 25 times more effective against bacteria than chlorhexidine and also have antiviral and antifungal properties [20]. The main objective of this research was to assess the hemocompatibility of Ag NP and its effects as an antimicrobial against a virulent isolate of Streptococcus mutans at various concentrations.

2. Materials and Methods

2.1 Sample Preparation

A container with 5 mL of deionized water and an 8 mM CTAB surfactant solution is shown in Figure 1. The Danyang Xinli Alloy company in China provided a square plate of 98 percent pure silver, which was placed at the bottom of the container and had a thickness of 2 mm. The 10 ns pulse width, 1064 nm wavelength, 5 Hz repetition rate, and 10 cm focal length of the Nd: YAG laser were used to focus on a silver target. Weighing the target before and after the ablation procedure allowed us to calculate the concentration of nanoparticles.

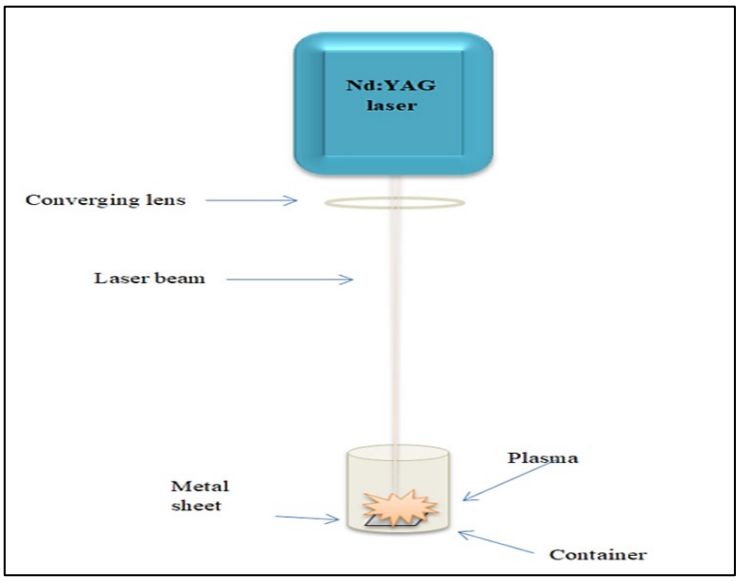

Figure 1: Schematic diagram of pulsed laser ablation

2.2 Characterization of Ag NPs

Optical, structural, and morphological techniques were used to characterize the generated Ag NPs. The absorption spectrum of Ag NPs in the spectral region (200-800 nm) was determined using a UV-VIS spectrophotometer (Shimadzu SP8001), as well as the composition and functional groups of the synthesized NPs Using a Fourier transform infrared (FTIR) spectrometer from PerkinElmer Spectrum Two/USA. The surface charge of nanoparticles was calculated using the Zeta potential, a measurement of electrostatic or charge repulsion or attraction between particles. XRD (Model XRD-6000, manufactured in Japan) was used to characterize the internal structure of synthesized NPs by dropping and drying an Ag NPs solution on an aluminium substrate at 2 angle = (20-80).

$$D=0.94\lambda/\beta\cos\theta \quad (1)$$

where λ is the wavelength of X-ray (1.54060 Å), β is the full width at half maximum of diffraction θ is the diffraction angle [23, 24].

The morphology and chemical composition of Ag NPs were recorded using field emission scanning electron microscopy and energy dispersive X-ray spectroscopy (FESEM; ZEISS SIGMA VP/Germany).

The size and morphology of Ag NPs were evaluated by using a transmission electron microscope (TEM) (ZEDSS LEO 912 AB-100KV) made in Germany. A drop of Ag NPs solution was deposited on a copper grid with a gold coating to prepare the TEM sample.

2.3 Antibacterial Activity Assay

Streptococcus mutans were activated in nutrient broth at 37°C for 24 hours with shaking incubation (300rpm) to reach the exponential phase (1× 106)CFU/mL. Five agar wells with 6-mm-diameter were filled with 100 µL of nanoparticle solutions at various concentrations (0.0, 25, 50, 100, and 200) µg/mL, and all Muller Hinton agar plates were incubated at 37ºC for 24 hrs. The inhibition rate was calculated for three replicates of the inhibition zone around the wells using the following Equation:

$$\text{Inhibition rate}\%=(1\text{-x-min})/(\text{max-min})\times 100\% \quad (2)$$

Whereas X= colony diameter at any concentration
Min = least inhibition zone
Max= biggest inhibition zone

2.4 Hemocompatibility Assay

A hemolysis assay of Ag, NPs prepared by laser ablation at various concentrations (0.0, 25, 75, 100, 200) g/mL was performed, as described elsewhere [25]. Human whole blood was collected via venous puncture from a healthy individual aged (25-35). Blood was collected in tubes containing anticoagulants (EDTA). 0.5mL of whole blood was mixed with 4.5mL of normal saline containing various concentrations of tested nano-metals, while DDW was used as a positive control (100 percent hemolysis), and normal saline was used as a negative control (0 percent hemolysis). All blood tubes were incubated at 37°C for 1 hour before being centrifuged at 3000 rpm for 5 minutes to measure absorbency using a UV-Vis spectrophotometer at 540 nm.

$$\text{Hemolysis } \% = (\text{Ab specimen} - \text{Ab control (- ve)}/\text{Ab control (+ ve)} - \text{Ab control (- ve)}) \times 100 \quad (3)$$

2.5 Statistical analysis

All data were statistically analyzed using the ANOVA test to express the significant differences at ($P < 0.05$) by using least significant differences (LSD).

3. Results and Discussion

3.1 Uv-Vis Assay

Using a UV-Vis absorption spectrophotometer (Shimatzu SP8001), the optical properties of the colloidal solution were measured. After the laser pulse shocked the submerged target, vapour formed on its surface. Focused plasma was produced after the surface layer absorbed laser pulses. Increasing the viscosity and density of the liquid brought the plasma closer to the surface of the silver plate during the laser ablation of an Ag target [26, 27]. Secondary ablation could occur, for example, if the contained plasma's high-pressure shockwaves etched the metal [28]. The absorption spectra of Ag NPs show an absorption peak in the vicinity of 425 nm. The temperature, pressure, and density of the plasma plume were increasing, resulting in an increase in peak intensity in all NP-containing solutions containing surfactants. As shown in Figure 2, surfactants increase the solvent density and viscosity, focusing the plasma at the Ag target's surface and increasing the efficiency with which Ag NPs are produced. The confined pressure at the surface of the silver plate could etch it via a secondary ablation process caused by the high-pressure shockwaves, resulting in the growth of more nanoparticles [27].

3.2 FTIR

The Fourier transform infrared (FTIR) technique is harnessed to investigate surfactant adsorption on the surface of metal nanoparticles and to determine the type of bonding vibrations [29]. Figure 3 shows the IR spectra of Ag-CTAB samples. The presence of Ag NPs structures bonding with oxygen from the hydroxyl group is indicated by vibration bands at 550 and 590 cm^{-1}, which validates the Ag NPs formulation. Broad absorption bands at around 2130 cm^{-1} are caused by carbon dioxide adsorbed on the sample's external surface as well as the C-H stretching vibration of the methyl and methylene groups [30]. The broad absorption peak at 3321 cm^{-1} is due to the stretching frequency of the -OH group in absorbed water because nanocrystal materials have a high surface-to-volume ratio and absorb moisture [27]. Besides, the band near 1630 cm^{-1} could well be hydroxyls (O-H) bending with Ag atoms [31].

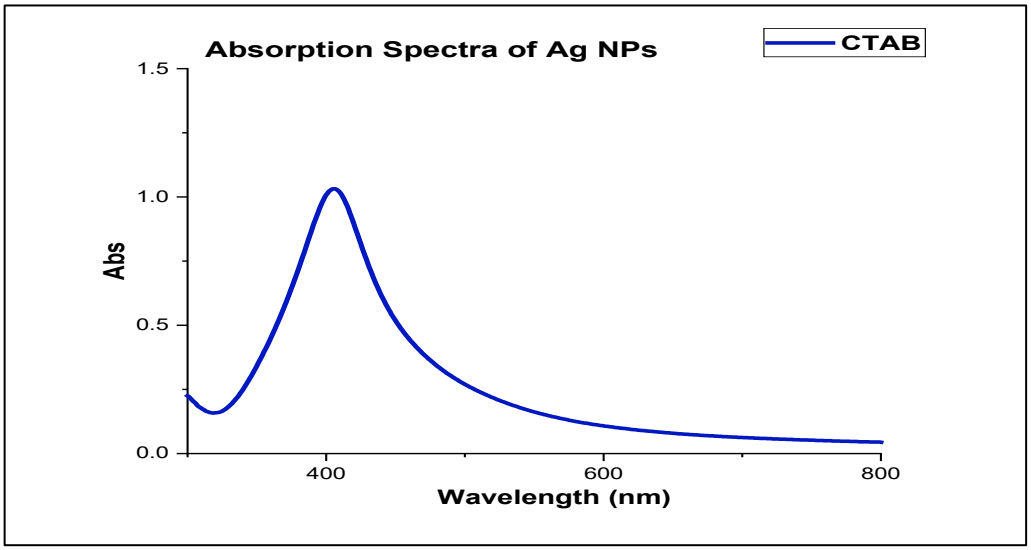

Figure 2: Absorption spectra of Ag NPs

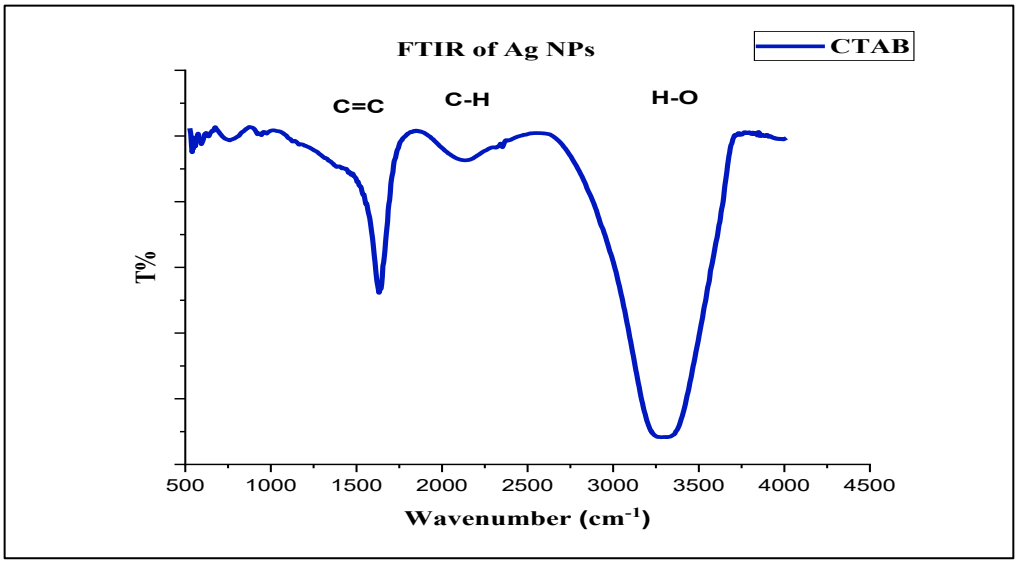

Figure 3: FTIR of Ag NPs with different solutions

3.3 Zeta potential

The zeta potential is a meaningful nanocrystal characterization tool for obtaining information on a surface charge, which can be used to evaluate the physical stability of a nanosuspension [29, 30]. Though since high ZP particles are highly charged, electrostatic repulsion prevents particle aggregation. When the ZP is low, attraction trumps repulsion, and the mixture agglomerates. The positive Zeta potential (ZP) peak distribution result obtained in the current work was 20 mV, as shown in Figures 4 (a) and (b). The physical stability of generated nanosuspensions could be influenced by material properties, the presence of surfactants, and the chemistry of the solution. Re-aggregation was reduced and surface coverage was enhanced when the positively charged surface of the nanoparticles was covered by surfactants such as CTAB [13, 32].

3.4 Structural Properties

The structural characterization of Ag NPs was probed using XRD. According to Card No. 04-0784, shown in Figure 5, all of the reflections coincided well with the cubic crystal phase of the Ag structure and matched the phase standard values of the plane of the Ag crystal. Table 1 contains a complete list of the XRD properties of Ag NPs. The exceptional crystallinity is owing to the sharpness and abundance of peaks in the XRD pattern. The crystalline size of NPs was determined using the Scherrer formula (C.s). Table 1 summarizes the XRD data for experimental Ag NPs, including peak position, crystalline size variation, FWHM, interplanar spacing (dhkl), and miller index (hkl)[33, 34].

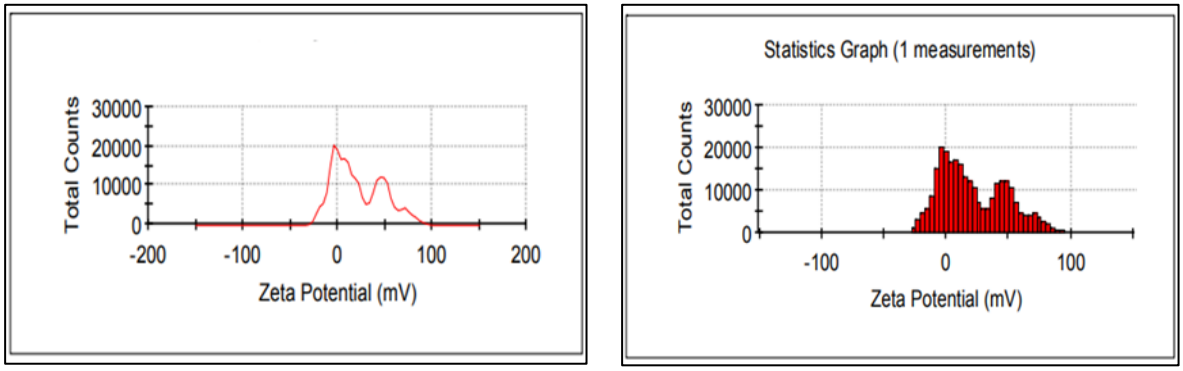

(a) **(b)**

Figure 4: a) Zeta potential of Ag NPs colloidal with CTAB and b) Zeta potential distribution of Ag NPs colloidal with CTAB

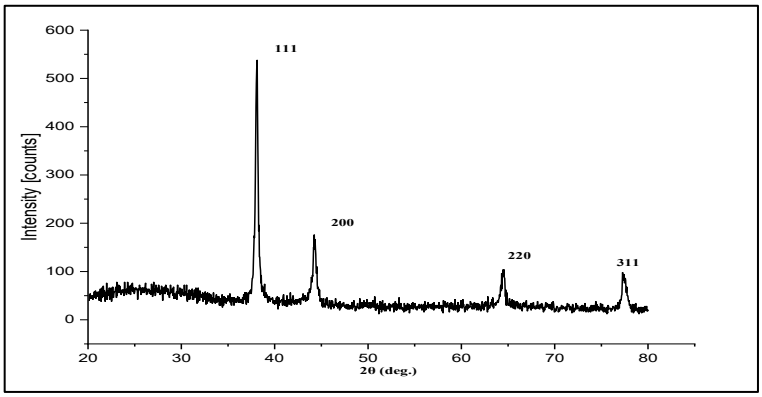

Figure 5: XRD of Ag NPs

Table 1: XRD of Ag NPs

2 θ (deg.)	FWHM (deg.)	d_{hkl}Exp. (A °)	CS (nm)	hkl	d_{HKL} STD	Material	Geometric Crystal system	Card number
37	0.54	2.42	15.52	111	2.3550	Silver	Cubic	04-0784
45	0.62	2.01	13.87	200	2.0390	Silver	Cubic	04-0784
69	0.59	1.36	16.34	220	1.4420	Silver	Cubic	04-0784
78	0.64	1.22	15.98	311	1.2300	Silver	Cubic	04-0784

3.5 TEM Imaging of Ag NPs

TEM was used to explore the particle size distribution and morphological properties of Ag NPs. Figures 6a and 6b displays the TEM image and particle size distribution of Ag NPs generated in a CTAB environment. where the TEM image showcases a spherical graphitic shape with a particle size distribution ranging from (5-70 nm) and a large percentage of NPs are close to one another, resulting in a chain-like pattern [31]. Previous research has shown that laser ablation generation of metal NPs in CTAB produces inhomogeneous particle-size NPs [35]. The size of CTAB surfactant nanoparticles was determined by the tension between successive particle development and CTAB coating [9]. Raising the CTAB concentration may keep improving the protection of Ag particles from Ag incorporation via diffusion by CTAB molecules. As a matter of fact, the particle surfaces were completely coated with CTAB surfactant molecules, preventing additional surface charge-induced development [13, 36, 37].

3.6 FESEM Imaging of Ag NPs

A FESEM pattern of Ag NPs generated in CTAB solution was determined, as shown in Figures 7 (a) and (b), respectively. Big particles are produced during the initial generation of nanoparticles from high-intensity laser pulses striking a silver target. Once the contact zone reaches its boiling point, it explodes, releasing nanodroplets and ionized materials onto the substrate [38]. These nanodroplets can solidify on the medium as ionized matter nucleates and grow, forming spherical micrometric and submicrometric particles that appear to form from the aggregation of fine nanoparticles [7, 39, 40]. As can be seen in Figure 7a, the EDS analysis confirms that even the microstructured particles are made of Ag. While Figure 7 (c) displays the energy dispersive spectrometer. CTAB also contained some aggregated nanoparticles, which is a common side effect of laser ablation due to the nanoparticle creation approach. Laser-ablated nanostructures have a spherical shape, according to FESEM images [17, 38]. As a result, CTAB surfactant was used to stabilize nanoparticles, protecting them from aggregation and other external influences [39].

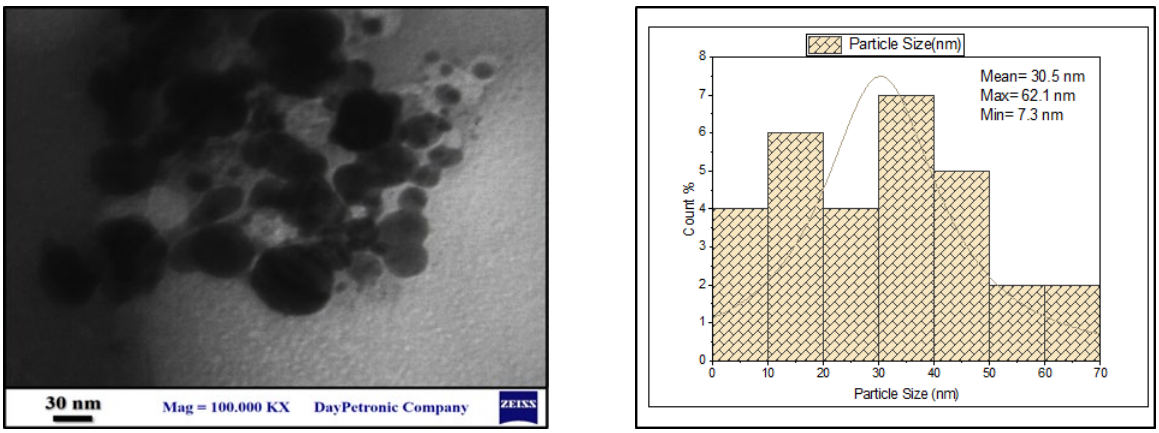

(a) **(b)**

Figure 6: a) Morphological properties of Ag NPs synthesized with CTAB and b) particle size distribution

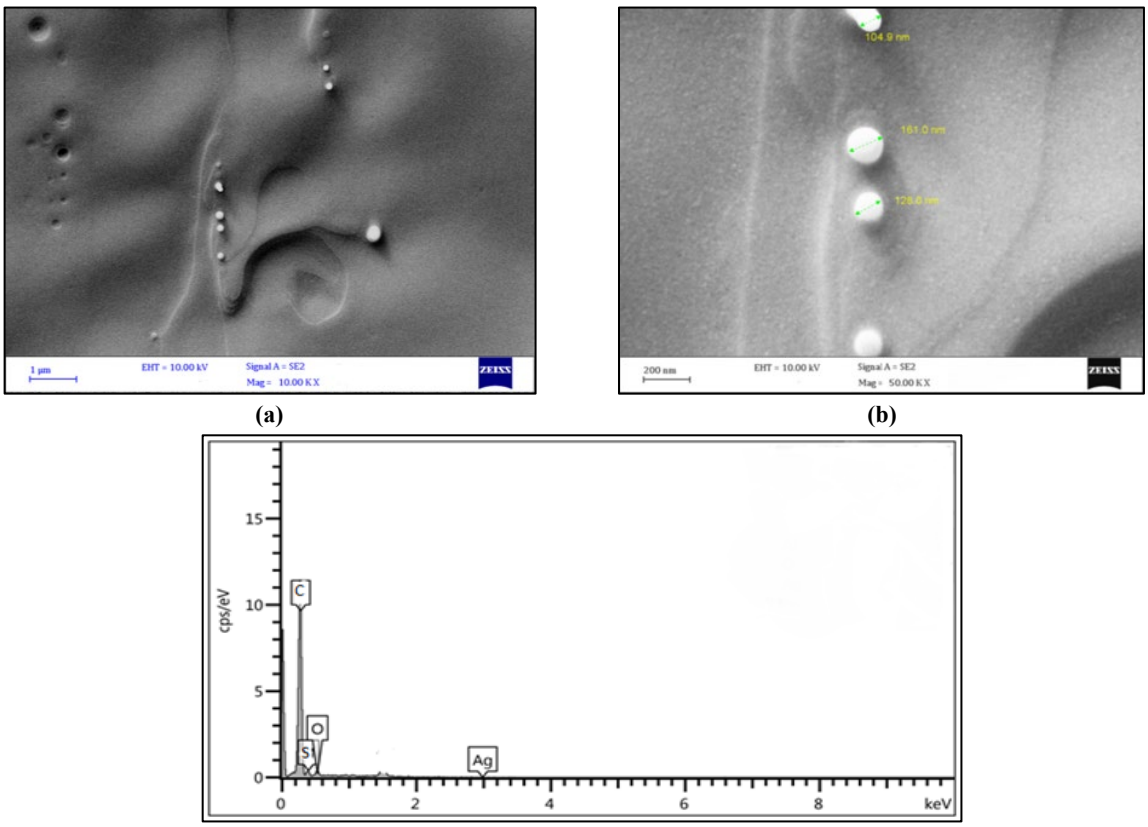

(a) **(b)**

(c)

Figure 7: FESEM images of Ag NPs synthesized in SDS a) FESEM at mag=10.00 KX, b) FESEM at mag=50.00 KX, and c) EDS

3.7 Antibacterial Assay

The antibacterial efficacy of various nanoparticle concentrations against Streptococcus mutans was assessed, and a good diffusion method was used to detect the presence of an inhibitory zone. it was found that as the concentrations of Ag NPs (0.0, 25, 50, 100, and 200) g/mL increased, so did the inhibitory zone widths. Figures 8 (a) and (b) show that Ag NPs kill bacteria at the concentration levels used and that these effects were indeed closely related to concentration with distinct gaps at (p0.05). Figure 8 revealed that Ag NPs prepared in CTAB are more effective antibacterial agents. Metallic nanoparticle interactions with DNA, lysosomes, ribosomes, and enzymes can result in oxidative stress, heterogeneous changes, abnormal cellular uptake, electrolyte imbalances, and protein deactivation [41]. Furthermore, Ag NPs can alter gene expression and impair enzyme performance. Metallic nanoparticles (MNs) and their ions generate superoxide radicals (ROS), causing oxidative stress in cells. Metallic nanoparticles dissolved and adhered to bacterial membranes, causing harm [21]. Silver ions (Ag+) can be released by silver nanoparticles adhering to or passing through cell walls and cytoplasmic membranes, disrupting both structures, according to the suggested killing mechanisms of (AgNPs). Silver ions can cause ribosome denaturation and thus halt protein production. Because silver ions render the respiratory enzyme on the cytoplasmic membrane inactive, ATP production is halted. Membrane disruption can be caused by reactive oxygen species. When the electron transport chain fails, reactive oxygen species are formed. Replication of deoxyribonucleic acid (DNA) is hampered in five ways: reactive oxygen species and silver inhibit cell growth by binding to deoxyribonucleic acid and preventing replication. The accumulation of silver nanoparticles in the pits of the cell wall induces membrane denaturation. Furthermore, electrostatic attraction between positively charged NPs and negatively charged bacterial cell surfaces is essential for NPs' activity as bactericidal agents and accounts for a significant portion of NPs' overall antibacterial activity [42]. The present study, like other studies, reveals that NPs cause mitochondrial and DNA damage, culminating in cell death. This is because cell death is caused by mitochondrial damage and the increase in the production of several apoptotic proteins. This caused a leak in the membrane and the release of the protein's driving force. Nanomaterials are also employed in orthodontic brackets, wires, and ligatures. Biofilms commonly occur in micro-implants and orthodontic retainers. While in deboning, orthodontic retainers containing Ag NPs showed considerable antibacterial activity against Streptococcus mutans [43].

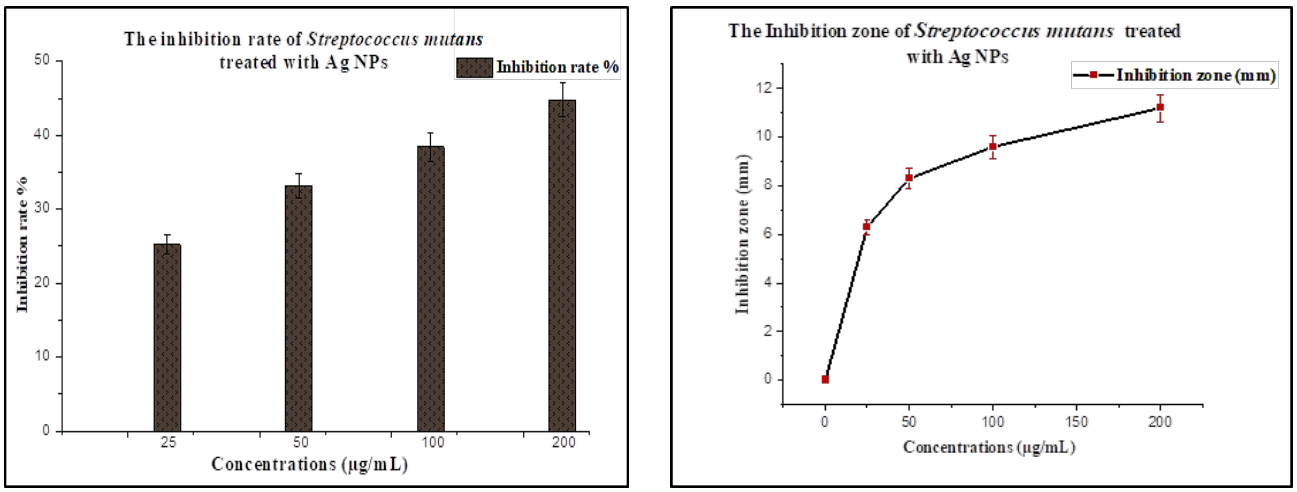

(a) **(b)**

Figure 8: (a) Inhibition rate (%) of streptococcus mutans treated with Ag NPs synthesized with CTAB, (b): The inhibition zone (mm) of prepared Ag NPs on Streptococcus mutans

3.8 Hemocompatibility Assay

Any therapeutic material should be biocompatible and have low hemolytic effects. As a result, as shown in Figure 9, hemolysis was investigated for all prepared nanoparticles at various concentrations (0.0-200 g/mL). Erythrocytes may be fragile cells due to their high content of unsaturated phospholipids in their membranes, as well as their high content of both oxygen and hemoglobin [32]. MNPs have been linked to several processes, including membrane integrity maintenance, changes in cell membrane proteins and lipids, and osmosis-induced changes in cell water content. There were more deficient effects on RBCs, causing cell membrane disintegration, over the tested lower concentration range of NPs [44, 45], and this impact was similar to that of the positive control. These findings revealed that NP concentrations ranged from 20 to 200 g/mL. In previous studies, NPs caused red blood cells to morphologically change from their typical discoid form to schistocytes, according to the bilayer couple theory [38]. Because of the unequal expansion of the two monolayers of the red cell membrane, foreign substances cause erythrocytes to change shape. When the chemical enters the inner monolayer, stomatocytes are formed, and when it enters the outer moiety, spiculated-shaped schistocytes are formed. The fact that pure RES stimulated the production of schistocytes suggests that it was introduced into the outer leaflet of the erythrocyte membrane [46].

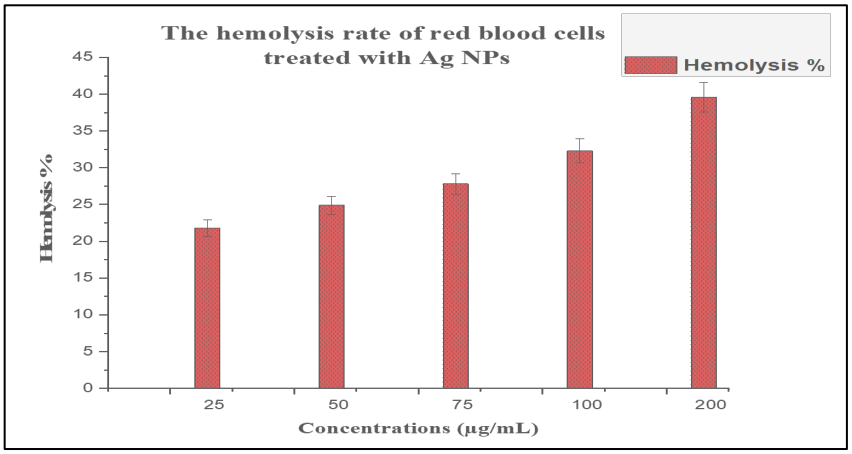

Figure 9: blood compatibility assay of red blood cells treated with Ag NPs synthesized by laser ablation in CTAB

4. Conclusion

The findings demonstrate that ablation with a Q-switched Nd:YAG laser (1064 nm, 600 mJ at room temperature, pulse duration of 10 ns, and repetition rate of 5 Hz) is capable of producing spherical graphitic Ag NPs with particle sizes ranging from 5-70 nm. The absorption spectrum of Ag NPs is approximately 425 nm. Ablation in CTAB liquids produces spherical Ag NPs. An in vitro assay revealed that prepared Ag NPs have significant antibacterial activity against Streptococcus mutans as well as moderate toxic effects at high concentrations, with the hemolysis rate of red blood cells increasing with Ag NP concentration.

Acknowledgment

Acknowledgments may be directed to individuals or institutions that have contributed to the research or a government agency.

Author Contribution

All authors contributed equally to this work.

Funding

This paper received no external funding

Data Availability Statement

The data that support the findings of this study are available on request from the corresponding author.

Conflicts of Interest

The author declares that there're no conflicts of interest for declaration.

References

[1] N. El-Desouky et al., Synthesis of silver nanoparticles using bio valorization coffee waste extract: photocatalytic flow-rate performance, antibacterial activity, and electrochemical investigation, Biomass Conv. Bioref., (2022) 1-15. https://doi.org/10.1007/s13399-021-02256-5

[2] M. Yazdanian et al., The Potential Application of Green-Synthesized Metal Nanoparticles in Dentistry: A Comprehensive Review, Bioinorg. Chem. Appl., 2022 (2022) 27. https://doi.org/10.1155/2022/2311910

[3] L. Fritea et al., Metal nanoparticles and carbon-based nanomaterials for improved performances of electrochemical (Bio) sensors with biomedical applications, Materials, 14 (2021) 6319. https://doi.org/10.3390/ma14216319

[4] A.C. Burdușel et al., Biomedical applications of silver nanoparticles: an up-to-date overview, Nanomater, 8 (2018) 681. https://doi.org/10.3390/nano8090681

[5] Agnihotri, S., and N.K. Dhiman. 2017. Development of nano-antimicrobial biomaterials for biomedical applications, in Advances in biomaterials for biomedical applications, Vol. 66, pp. 479-545. Springer. https://doi.org/10.1007/978-981-10-3328-5_12

[6] Tabatabaei, F.S., R. Torres, L. Tayebi. 2020. Biomedical materials in dentistry. Applications of Biomedical Engineering in Dentistry, pp. 3-20. https://doi.org/10.1007/978-3-030-21583-5_2

[7] J. Jeevanandam et al., Review on nanoparticles and nanostructured materials: history, sources, toxicity and regulations, Beilstein J. Nanotechnol., 9 (2018) 1050-1074. https://doi.org/10.3762%2Fbjnano.9.98

[8] T.V. Duncan, Applications of nanotechnology in food packaging and food safety: barrier materials, antimicrobials and sensors, J. Colloid Interface Sci., 363 (2011) 1-24. https://doi.org/10.1016/j.jcis.2011.07.017

[9] M.S. Chavali, M.P. Nikolova, Metal oxide nanoparticles and their applications in nanotechnology, SN Appl. Sci., 1 (2019) 1-30. https://doi.org/10.1007/s42452-019-0592-3

[10] A. Hamad, L. Li, Z. Liu, A comparison of the characteristics of nanosecond, picosecond and femtosecond lasers generated Ag, TiO2 and Au nanoparticles in deionised water, Appl. Phys. A ,120 (2015) 1247-1260. https://doi.org/10.1007/s00339-015-9326-6

[11] A.M. Haleem et al., Cytotoxic effects of titanium dioxide nanaoparticles synthesized by laser technique on peripheral blood lymphocytes and hep-2 Cell Line, Toxicol. Environ. Health Sci., 11 (2019) 219-225. https://doi.org/10.1007/s13530-019-0407-3

[12] R.M. Altuwirqi, Graphene Nanostructures by Pulsed Laser Ablation in Liquids: A Review, Materials, 15 (2022) 5925. https://doi.org/10.3390/ma15175925

[13] Y.-H. Chen, C.-S. Yeh, Laser ablation method: use of surfactants to form the dispersed Ag nanoparticles, Colloids Surf. A, 197 (2002) 133-139. https://doi.org/10.1016/S0927-7757(01)00854-8

[14] H. Hassan et al., Gold nanomaterials–The golden approach from synthesis to applications, Mater. Sci. Energy Technol., 5 (2022) 375-390. https://doi.org/10.1016/j.mset.2022.09.004

[15] F. Lavaee et al., The Effect of Gold Nano Particles with Different Sizes on Streptococcus Species, J. Dent., 22 (2021) 235–242. https://doi.org/10.30476%2FDENTJODS.2021.85219.1119

[16] L. Gao et al., Nanocatalysts promote Streptococcus mutans biofilm matrix degradation and enhance bacterial killing to suppress dental caries in vivo, Biomater, 101 (2016) 272-284. https://doi.org/10.1016/j.biomaterials.2016.05.051

[17] A. O. El-Gendy et al., The antimicrobial effect of 400 nm femtosecond laser and silver nanoparticles on Gram-positive and Gram-negative bacteria, J. Photochem. Photobiol. B, 223 (2021) 112300. https://doi.org/10.1016/j.jphotobiol.2021.112300

[18] J. Hadi, S. Wu, G. Brightwell, Antimicrobial blue light versus pathogenic bacteria: mechanism, application in the food industry, hurdle technologies and potential resistance, Foods, 9 (2020) 1895. https://doi.org/10.3390/foods9121895

[19] J.T. Seil, T.J. Webster, Antimicrobial applications of nanotechnology: methods and literature, Int. J. Nanomed., 7 (2012) 2767. https://doi.org/10.2147%2FIJN.S24805

[20] F.M. Omar, H.A. Aziz, S. Stoll, Aggregation and disaggregation of ZnO nanoparticles: influence of pH and adsorption of Suwannee River humic acid, Sci. Total Environ., 468-469 (2014) 195-201. https://doi.org/10.1016/j.scitotenv.2013.08.044

[21] E. Omurzak et al., Effect of surfactant materials to nanoparticles formation under pulsed plasma conditions and their antibacterial properties, Mater. Today: Proc., 5 (2018) 15686-15695. https://doi.org/10.1016/j.matpr.2018.04.179

[22] T.H. Ong et al., Cationic chitosan-propolis nanoparticles alter the zeta potential of S. epidermidis, inhibit biofilm formation by modulating gene expression and exhibit synergism with antibiotics, PLoS One, 14 (2019). https://doi.org/10.1371/journal.pone.0213079

[23] A.M. Haleem, A. Kadhim, R.H. Abbas, Antibacterial activity of copper oxide nanoparticles against Escherichia coli ATCC 25922 and Staphylococcus aureus ATCC 25923, Adv. Nat. Appl. Sci., 11 (2017) 1-5.

[24] Cervellino, A., et al. 2016. X-ray powder diffraction characterization of nanomaterials, in X-ray and neutron techniques for nanomaterials characterization. pp. 545-608. Springer. https://doi.org/10.1007/978-3-662-48606-1_10

[25] A.A. Al-Jubori, G.M. Sulaiman, A.T. Tawfeeq, Antioxidant Activities of Resveratrol Loaded Poloxamer 407: An In Vitro and In Vivo Study, J. Appl. Sci. Nanotechnolo., 1 (2021) 1-12. http://dx.doi.org/10.53293/jasn.2021.3809.1046

[26] H. A. Kazem, and M. T. Chaichan, Effect of humidity on photovoltaic performance based on experimental study, Int. J. Appl. Eng., 10 (2015) 43572-43577.

[27] T. Tsuji et al., Preparation of silver nanoparticles by laser ablation in polyvinylpyrrolidone solutions, Appl. Surf. Sci., 254 (2008) 5224-5230. https://doi.org/10.1016/j.apsusc.2008.02.048

[28] S.S. Mao et al., Influence of preformed shock wave on the development of picosecond laser ablation plasma, J. Appl. Phys., 89 (2001) 4096-4098. https://doi.org/10.1063/1.1351870

[29] M. Hafizah, A. Riyadi, A. Manaf, Particle size reduction of polyaniline assisted by anionic emulsifier of sodium dodecyl sulphate (SDS) through emulsion polymerization, IOP Conference Series: Materials Science and Engineering, 515,2019, 012080. https://doi.org/10.1088/1757-899X/515/1/012080

[30] Ramimoghadam, D., M.Z.B. Hussein, Y.H. Taufiq-Yap, The effect of sodium dodecyl sulfate (SDS) and cetyltrimethylammonium bromide (CTAB) on the properties of ZnO synthesized by hydrothermal method, Int. J. Mol. Sci., 13 (2012) 13275-13293. https://doi.org/10.3390/ijms131013275

[31] S. Sun, A. Wang, Adsorption kinetics of Cu (II) ions using N, O-carboxymethyl-chitosan, J. Hazard. Mater., 131 (2006) 103-111. https://doi.org/10.1016/j.jhazmat.2005.09.012

[32] Z. Sui et al., Capping effect of CTAB on positively charged Ag nanoparticles, Physica E Low Dimens. Syst. Nanostruct., 33 (2006) 308-314. https://doi.org/10.1016/j.physe.2006.03.151

[33] B. Gogoi et al., Facile biogenic synthesis of silver nanoparticles (AgNPs) by Citrus grandis (L.) Osbeck fruit extract with excellent antimicrobial potential against plant pathogens, SN Appl. Sci., 2 (2020) 1-7. https://doi.org/10.1007/s42452-020-03529-w

[34] Anandalakshmi, K., J. Venugobal, and V. Ramasamy, Characterization of silver nanoparticles by green synthesis method using Pedalium murex leaf extract and their antibacterial activity, Appl. Nanosci., 6 (2016) 399-408. https://doi.org/10.1007/s13204-015-0449-z

[35] A. Subhan, A.-H.I. Mourad, Y. Al-Douri, Influence of Laser Process Parameters, Liquid Medium, and External Field on the Synthesis of Colloidal Metal Nanoparticles Using Pulsed Laser Ablation in Liquid: A Review, Nanomater, 12 (2022) 2144. https://doi.org/10.3390/nano12132144

[36] F. Mafuné et al., Structure and stability of silver nanoparticles in aqueous solution produced by laser ablation, J. Phys. Chem. B, 104 (2000) 8333-8337. https://doi.org/10.1021/jp001803b

[37] M. Moradi et al., Effect of aqueous ablation environment on the characteristics of ZnO nanoparticles produced by laser ablation, J. Clust .Sci., 27 (2016) 127-138. https://doi.org/10.1007/s10876-015-0915-5

[38] S.H. Sabeeh, H.A. Hussein, H.K. Judran, Synthesis of a complex nanostructure of CuO via a coupled chemical route, Mater. Res. Express., 3 (2016) 125025. https://doi.org/10.1088/2053-1591/3/12/125025

[39] Pavithra, K., M. Yashoda, S. Prasannakumar, Synthesis characterisation and thermal conductivity of CuO-water based nanofluids with different dispersants, Part. Sci. Technol., 38 (2019) 559-567. https://doi.org/10.1080/02726351.2019.1574941

[40] D. Liyanage et al., An analysis of nanoparticle settling times in liquids, J. Nanomater., 2016 (2016) 44. https://doi.org/10.1155/2016/7061838

[41] H. Jang et al., Antibacterial properties of cetyltrimethylammonium bromide-stabilized green silver nanoparticles against methicillin-resistant Staphylococcus aureus, Arch. Pharm. Res., 38 (2015) 1906-1912. https://doi.org/10.1007/s12272-015-0605-8

[42] A. Gupta et al., Combatting antibiotic-resistant bacteria using nanomaterials, Chem. Soc. Rev., 48 (2019) 415-427. https://doi.org/10.1039/C7CS00748E

[43] L. Gabrielyan, A. Trchounian, Antibacterial activities of transient metals nanoparticles and membranous mechanisms of action, World J. Microbiol. Biotechnol., 35 (2019) 1-10. https://doi.org/10.1007/s11274-019-2742-6

[44] G. Lim HW, M. Wortis, R. Mukhopadhyay, Stomatocyte–discocyte–echinocyte sequence of the human red blood cell: Evidence for the bilayer–couple hypothesis from membrane mechanics, Proc. Natl. Acad. Sci., 99 (2002) 16766-16769. https://doi.org/10.1073/pnas.202617299

[45] J. Choi et al., Physicochemical characterization and in vitro hemolysis evaluation of silver nanoparticles, Toxicol. Sci., 123 (2011) 133-143. https://doi.org/10.1093/toxsci/kfr149

[46] M. Suwalsky, F. Villena, M. Gallardo, In vitro protective effects of resveratrol against oxidative damage in human erythrocytes, Biochim. Biophys. Acta Biomembr., 1848 (2015) 76-82. https://doi.org/10.1016/j.bbamem.2014.09.009